ELSEVIER

Contents lists available at ScienceDirect

International Journal of Biological Macromolecules

journal homepage: www.elsevier.com/locate/ijbiomac

A biodegradable poly-L-lactic acid (PLLA)/polybutylene adipate-*co*-terephthalate (PBAT) composite aerogel for continuous oil-water separation

Xinkai Suna, Xinying Jianga, Fei Xiea, Pengju Yaoa, Yi Zhanga, Hui Yangb, Carla Bittencourtc, Wenjiang Lia,*

- a School of Materials Science and Engineering, School of Chemistry and Chemical Engineering, Tianjin University of Technology, Tianjin, 300384, China
- b Zhejiang-California International Nanosystems Institute, Zhejiang University, Hangzhou, 318000, China
- c Chimie des Interactions PLLAsma-Surface, Universit'e de Mons (UMONS), 20 PLLAce du Parc, Mons, 7000, Belgium

ARTICLE INFO

Keywords: PLLA PBAT Aerogel Biodegradability Oil-water separation

ABSTRACT

In the context of sustainable development, the exploration of renewable, biodegradable, and environmentally friendly polymer aerogels have emerged as a significant area of research. Herein, we report a facile synthesis of fully degradable polylactic acid (PLLA)/poly (butylene adipate-co-terephthalate) (PBAT) composite aerogels via 1,4-dioxane-assisted co-dissolution, followed by freeze-drying and phase separation techniques. The resulting aerogels feature a hierarchically porous structure with 98.6% porosity and vertically aligned channels, formed by controlled solvent crystallization during the freezing process. This unique architectural configuration integrates PLLA's oil-retention capability with PBAT's elasticity, yielding adsorption capacities of 13.6 g/g for n-hexane and 31.5 g/g for carbon tetrachloride. Notably, the aerogel retains ~97.5% stress and height recovery after 100 cycles of 50% strain compression, overcoming pure PLLA's inherent brittleness. It also maintains 96.5% the oil-water separation efficiency after 20 c centrifugal desorption cycles. 1,4-Dioxane promotes the compatibility of PLLA and PBAT, improving the interfacial compatibility and effectively avoiding the structural defects usually caused by phase separation. This research provides a scalable, filler-free approach to fabricate the high-performance biodegradable aerogels, bridging environmental sustainability and practical functionality for oily wastewater remediation.

1. Introduction

In recent years, persistent discharge of industrial oily wastewater and frequent oil and organic matter spills have caused serious ecological damage, particularly in marine environments, leading to substantial economic losses worldwide [1]. Conventional oil-water separation techniques, such as microbial degradation, physical methods (e.g., centrifugation and adsorption), and chemical treatments (e.g., dispersants and combustion), often exhibit limitations, including low efficiency, high energy consumption, and secondary pollution, which restrict their practical applicability [2–5]. Among these methods, adsorption-based technologies are widely recognized as the most effective for oil-water separation due to their scalability, environmental friendliness, and absence of harmful byproducts [6]. In particular, aerogels, a class of solid materials characterized by ultra-low density, high

porosity, and large specific surface area, have attracted significant attention in recent years. Owing to their unique chemical and physical properties, aerogels have been applied in diverse fields, including aerospace, thermal insulation, soundproofing, electronics, adsorption separation, and catalysis [7–11]. Polymer-based aerogels, in particular, offer advantages such as low cost, high processability, and adjustable morphology, making them suitable for a wide range of applications [12–17]. However, a major limitation of most polymer-based aerogels is their reliance on petroleum-derived polymers during synthesis. The non-biodegradability of these polymers has become a mounting concern, exacerbating the global energy crisis and contributing to microplastic pollution throughout their lifecycle [18]. As environmental awareness and demand for sustainable solutions grow, there is an urgent need to develop green, straightforward, and cost-effective methods for producing degradable aerogels.

* Corresponding author at: School of Materials Science and Engineering, Tianjin University of Technology, Tianjin, 300384, China. E-mail address: liwj@tjut.edu.cn (W. Li).

Recently, the development of bio-based materials, such as poly(lactic acid) (PLLA) and poly(butylene adipate-co-terephthalate) (PBAT), has attracted significant interest in sustainable adsorption technologies [19,20]. PLLA, derived from renewable resources such as corn starch, is biodegradable, biocompatible, and mechanically robust, making it ideal for aerogel matrices [21]. PBAT, on the other hand, exhibits excellent flexibility and elongation at break, complementing the rigidity of PLLA. Nevertheless, PLLA aerogels face three major challenges that limit their applications: relatively low adsorption capacity, poor pore structure, and poor compression recovery, all of which affect their reusability [22–24]. To address these limitations and improve the performance of PLLA aerogels, various strategies have been explored, including the incorporation of fillers such as SiO2 [25,26], glass fibers [27], carbon nanotubes [28-30], and ZIF nanoparticles [13,31,32]. Zhang et al. reduced the energy loss coefficient of PLA aerogels from 54% to 31%after 100 compression cycles via ZrO2 incorporation; the maximum stress only slightly decreased from the initial 5.66 kPa to 5.25 kPa after the same number of cycles [33]. Naveed Iqbal et al. incorporated

AgNPs into the aerogel, which retained 81.25% of its original compressive stress (2.6 kPa) after 100 cycles, with 90% of its original Young's modulus preserved and the energy loss coefficient reduced from 61.5% to 48.8% [34].

However, these approaches typically entail complex synthesis procedures, costly precursors, or incorporation of non-degradable components, thereby increasing environmental burdens [35,36]. A more sustainable solution lies in polymer blending technology, which combines PLLA and PBAT to integrate their inherent merits. However, the compatibility between PLLA and PBAT is inherently poor due to their distinct chemical structures and substantial differences in solubility parameters (δ). Specifically, PLLA has a δ value of approximately 10.1 (cal/cm3)1/2, whereas PBAT's δ is approximately 23.0 (cal/cm3)1/2. This mismatch drives phase separation, preventing the formation of homogeneous aerogels.

To overcome this insolubility and achieve the homogeneous mixing required for aerogel fabrication, a versatile solvent capable of *co*-dissolving both polymers is essential. Remarkably, 1,4-dioxane has been identified as an effective solvent for co-dissolving PLLA and PBAT, enabling molecular-level mixing through hydrogen bonding with carbonyl groups while reducing interfacial energy [37]. During freezedrying, 1,4-dioxane crystallizes prior to polymer aggregation, inducing the formation of vertically aligned pores, preventing structural collapse, and enhancing both specific surface area and pore connectivity [10,38]. Notably, no prior studies have reported the use of 1,4-dioxane for codissolving PLLA and PBAT in aerogel fabrication, particularly for applications in petroleum contaminant adsorption. This solvent-enabled strategy eliminates the need for fillers, simplifying preparation and preserving the biodegradability of the composite.

In this study, we report a scalable, filler-free fabrication method for PLLA/PBAT composite aerogels via direct freeze-drying and phase separation, using 1,4-dioxane as a co-solvent. The resulting aerogels exhibit a dendritic structure with vertically aligned channels, formed through controlled solvent crystallization. Optimizing the PLLA/PBAT ratio enhances oil adsorption capacity (via improved porosity and surface hydrophobicity) and compression resilience (through PBAT-mediated interchain interactions), thereby improving reusability. Comprehensive evaluations of adsorption kinetics, surface properties, mechanical resilience, and reusability demonstrate the practical potential of these aerogels for oil spill remediation and oily wastewater treatment. This work provides a green alternative to filler-modified aerogels, addressing critical gaps in sustainable environmental materials.

2. Experimental section

2.1. Materials

Poly (lactic acid) (PLLA, L:D = 95:5 high-gloss grade, Mw = 80,000

g/mol) was purchased from COFCO Biotechnology Co., Ltd. (China). Poly (butylene adipate-co-terephthalate) (PBAT, high-gloss grade, Mw = 120,000 g/mol) was supplied by Xinjiang Lanshan Tunhe Polyester Co., Ltd. (China). 1,4-Dioxane (analytical reagent, purity >99.5%) was obtained from Aladdin Biochemical Technology Co., Ltd. (China). Organic solvents and oils, including methylene blue, Sudan I, acetone ($\geq$ 99.5%), carbon tetrachloride ($\geq$ 99.0%), toluene ($\geq$ 99.5%), n-hexane ($\geq$ 95.0%), olive oil, pump oil, and 18# gear oil, were purchased from Tianjin Fengchuan Chemical Reagent Factory (China) and used as received without further purification.

2.2. Preparation of PLLA and PBAT composite aerogels

The PLLA/PBAT composite aerogels were fabricated via a solvent-induced phase separation and freeze-drying method as follows: (1) A total of 1.5 g of PLLA/PBAT blends (with mass ratios of 100:0, 70:30, 50:50, 30:70, and 0:100) were added to 50 mL of 1,4-dioxane. The mixture was magnetically stirred (400 rpm) at 60 ± 1 °C for 4 h to ensure complete dissolution, forming a homogeneous precursor solution. (2) The homogeneous solution was poured into cylindrical Teflon molds (Φ 15 mm $\times$ 20 mm) and frozen at -20 ± 0.5 °C for 24 h to induce solvent crystallization and polymer phase separation. (3) The homogeneous solution Freeze-Drying: The frozen samples were transferred to a freeze dryer (FD-1 A-50, Beijing Boyikang

Laboratory Instrument Co., Ltd.) and dried at -20 °C under a vacuum of 1 ± 0.1 Pa for 24 h to sublimate the solvent, yielding porous aerogels. The resulting aerogels were labeled PBAT-x, where x denotes the weight percentage of PBAT in the blend (e.g., PBAT-30% corresponds to 30 wt% PBAT and 70 wt% PLIA).

2.3. Characterizations and measurements

The morphology of the composite samples was characterized by scanning electron microscopy (SEM, Thermo Fisher Scientific Quanta FEG 250). X-ray diffraction (XRD, Rigaku Ultima IV) was used to analyze the crystal structure. Surface functional groups were identified via Fourier transform infrared spectroscopy (FTIR) in the 500–4000 cm-1 range using a Frontier Mid-IR FTIR/STA6000-TL9000-Clarus SQ8 (Perkin Elmer, USA). Pore properties were determined by vacuum impregnation with anhydrous ethanol, calculating the pore volume based on the mass difference before and after impregnation using the following equation:

Porosity% =

$$(V_0 - V_1)/V_0 \times 100\%$$

(1)

V_1 – the absolute dense volume of the material, cm3 , V_0 – the volume of the material in its natural state, or apparent volume, cm3.

Compression tests were evaluated on a universal testing machine (MTS SYSEMS, CMT6502), equipped with a 50 N load cell, operating at a crosshead speed of 6 mm/min. The water contact angle (WCA) values were measured at three different positions on the sample using a KRUSS DSA100 optical system and averaged. The water droplets in the test were 2.0 μ L [39].

2.4. Oil adsorption performance and reusability test

To evaluate the adsorption capacity of PLLA/PBAT composite aerogels for various oils and organic solvents, a pre-weighed aerogel sample was immersed in the target liquid at room temperature. For non-volatile liquids (e.g., olive oil, gear oil), the sample was allowed to stand until adsorption equilibrium was reached; for volatile solvents (e.g., hexane, toluene), the immersion was performed quickly to minimize solvent evaporation. After adsorption, the aerogel was carefully removed, PLLAced on filter paper to drain excess liquid, and weighed immediately. The adsorption capacity (Q, g/g) was calculated using the mass difference before and after adsorption, and each test was repeated three times for reproducibility:

$$Q = (M_1 - M_0)/M_0 (2)$$

In this study, the adsorption capacity of PLLA/PBAT composite aerogel is denoted by Q, while M0 and M1 represent the weight of PLLA/PBAT composite aerogel before and after the adsorption of oil or organic solvents, respectively. It is important to note that all adsorption data were subjected to rigorous analysis, including three independent tests, and the results were subsequently averaged to ensure reliability and reproducibility.

The reusability of the PLLA/PBAT composite aerogel was evaluated using hexane as a representative oil and organic solvent. The removal of adsorbed oil or organic solvents from the aerogel was achieved through a combination of mechanical squeezing and distillation. These operations were repeated 20 times to determine the reusability of the PLLA/ PBAT composite aerogel.

Extrusion: Initially, the PLLA/PBAT composite aerogel was immersed in hexane until it reached saturated with adsorption. Subsequently, the aerogel was removed from the hexane solution and compressed to 80% of its original volume to expel the adsorbed hexane. The compressed PLLA/PBAT composite aerogel was then re-immersed in the hexane solution for further adsorption. During each cycle, the mass of the aerogel was carefully measured and recorded before and after hexane adsorption.

Distillation: Complete removal of hexane adsorbed to the PLLA/ PBAT composite aerogel was achieved through vacuum drying at 60 ◦C for 30 min. In each cycle, the mass of the aerogel before and after the adsorption was meticulously recorded to evaluate its adsorption capacity and reusability.

2.5. Continuous oil/water separation capability tests

Continuous separation of n-hexane/water (light oil) and carbon tetrachloride (CCl□)/water (heavy oil) mixtures was evaluated using a custom-built gravity-driven system. The apparatus consisted of a glass separator (50 mL capacity) and a filtration module: a PLLAstic dropper (inner diameter = 25 mm) packed with the PLLA/PBAT composite aerogel as the filtering layer (effective thickness = 5 mm).

2.5.1. Light oil (n-hexane) separation

A 20 mL mixture of n-hexane (dyed with Sudan I, 10 mL) and deionized water (dyed with methylene blue, 10 mL) was poured into the separator. The separator was tilted at 60◦ to direct the mixture toward the filtration module, where the aerogel selectively adsorbed n-hexane while repelling water. The separated n-hexane was collected in a graduated cylinder PLLAced beneath the dropper, relying solely on gravity (no external pressure).

2.5.2. Heavy oil (CCl□) separation

A 20 mL mixture of CCl□ (10 mL) and deionized water (10 mL) was used, with CCl□ naturally settling to the bottom (below water) due to its higher density. The mixture was introduced into the separator, and CCl□ was driven through the aerogel by gravity, with the effluent collected in a graduated cylinder.

For both light- and heavy-oil systems, the separation process was allowed to proceed until no further liquid outflow was observed. The oil flow rate (F, L/m2 h) is calculated using the following formula:

$$F = V/(St) \tag{3}$$

Where S denotes the effective separation area of the PLLA/PBAT composite aerogel layer, V is the volume of separated oil (L), and t is the filtration time.

Following the completion of the separation process, the mass of the separated water was measured, and the mass of the separated hexane (CCl4) was determined as the separation efficiency. The separation efficiency (R) was then calculated using the following formula:

$$R = \frac{m_1}{m_0} \times 100\% \tag{4}$$

where m0 and m1 are the weights of hexane (CCl4) before and after separation, respectively.

Then, the separated n-hexane (CCl4) was mixed with water again, and the procedure was repeated 10 times.

2.5.3. Cycling stability test

To evaluate the reusability of the PLLA/PBAT composite aerogel, the separated oil (n-hexane or CCl□) was re-mixed with fresh water to recreate a 20 mL oil/water mixture. The separation process was then repeated over 20 consecutive cycles. Following each cycle, the aerogel was thoroughly rinsed with ethanol (95 wt%) to remove residual oil, then dried at 60 ◦C for 2 h to remove any remaining oil before reuse.

3. Results and discussion

3.1. Fabrication and characterization of PLLA/PBAT composite aerogels

The PLLA/PBAT composite aerogels were synthesized via solventinduced phase separation, leveraging 1,4-dioxane's unique ability to dissolve PLLA and PBAT simultaneously. As schematically illustrated in Fig. 1a, the fabrication process involves three essential steps: (1) homogeneous dissolution of PLLA/PBAT blends in 1,4-dioxane at 60 ◦C, (2) freeze-curing at − 20 ◦C to induce solvent crystallization and polymer phase separation, and (3) freeze-drying to sublimate the solvent, yielding aerogels with interconnected porous networks. This approach circumvents the phase separation challenges typically encountered in PLLA/PBAT blends, as 1,4-dioxane facilitates hydrogen bonding between the carbonyl groups of the two polymers, thereby enhancing molecular compatibility [37]. (See Table 1.)

Digital photographs of the resulting aerogels (Fig. 1b) show that pure PLLA aerogel is brittle and white, while pure PBAT aerogel is flexible. The composite aerogels (PBAT-30%, PBAT-50%, PBAT-70%) exhibit intermediate optical properties, indicating successful blending. Notably, all aerogels retain structural integrity across different scales (from 1 cm to 5 cm diameter), demonstrating the scalability of the fabrication process. The ultra-lightweight nature of the composite aerogels is highlighted in Fig. 1c, where a PBAT-50% aerogel (density: 0.015 g/ cm3) is shown resting stably on flower petals without causing deformation. The high porosity of these aerogels is critical for adsorption applications, as it provides abundant voids for oil storage [7,38].

Scanning electron microscopy (SEM) was employed to examine the surface and cross-sectional morphologies of aerogels with varying PLLA/PBAT ratios, revealing the influence of PBAT content on the porous structures (Fig. 2a–i). The pure PLLA aerogel exhibits a welldefined, honeycomb-like 3D porous network with interconnected microscale pores, along with nanoscale pores (50–200 nm) on the pore

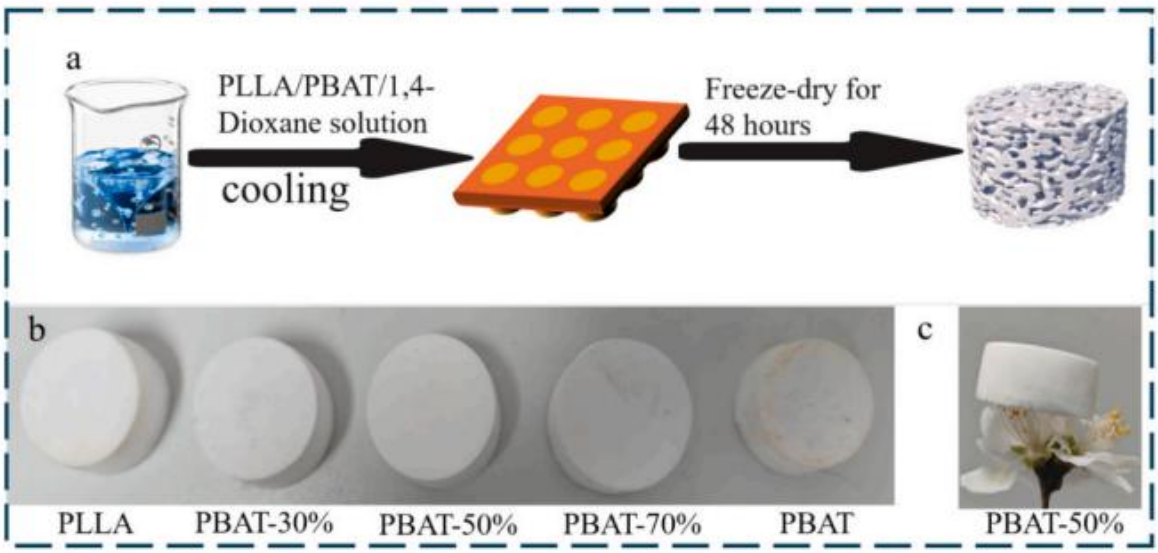

Fig. 1. (a) Schematic diagram of the preparation of PLLA/PBAT composite aerogel. (b) Digital photographs of PLLA, PBAT aerogel at various scales (c) PBAT addition at 50% supported by petals without deformation.

Table 1 Comparison of the properties of different porous materials.

Sorption materials	Raw Materials	AdsorptionCapacity [g/g]	Ref.
m-LA/PLLA foam	Polylactic acid Alkalinelignin	5.17–12.44	[42]
CPLLA/PBAT blended foam	PLLA, CE, and PBAT	3.8–11.2	[43]
PLLA foam	Polylactic acid	2-4	[51]
PVDF aerogel	Poly (vinylidene fluoride)	3–7	[52]
PP/PBMA-co-HEMAnonwoven	PPPBMA-co-HEMA	7–10	[53]
PP/PTFE foam	PPmnPTFE	4.6–9.1	[47]
Superhydrophobic polymer foams	PLLA	12–31	[48]
PLLA/hybrid fibers	PLLA, MoS2 and WS2	17.34-22.45	[49]
ZIF-8/PLLA compositeaerogel	PLLA Zinc nitrate hexahydrate 2-methylimidazole	15–30	[50]
ZIF-67@PLLA	PLLA	15-30	[1]
honeycomb aerogel	Cobalt hexahydrate nitrate		
Anisotropicallystructuredhydrophobic fungusaerogels	Pleurotus eryngiiMethyltrimethoxysila-neoctadecyltrichlorosilane	30	[54]
Superhydrophobic polymer foams	PLADioxane	13–31.5	[48]
(PLA/WO3/N-CQDs)	Polylactic acid	35.752	[55]
fibers	Sugarcane bagasseChloroform	33.732	[55]
PLLA/PBAT composite	PLLA	13.6-31.5	This
aerogels	PBAT		work

walls (Fig. 2a–c). This structure is attributed to directional crystallization of 1,4-dioxane during freezing, which acts as a temPLLAte for polymer assembly into ordered channels [38]. At 30 wt% PBAT (PBAT-30%, Fig. 2g), the honeycomb framework remains intact, but the pore walls become slightly fragmented, and the average pore diameter decreases to 15–35 μ m. This is due to the flexible aliphatic chains of PBAT partially filling the gaps between PLLA crystallites, thereby reducing surface irregularities. The PBAT-50% aerogel (Fig. 2d–f) exhibits an optimal morphology, maintaining the microscale honeycomb network (15–40 μ m pores) and nanoscale pores on the walls. This hierarchical

structure (micro- and nanopores) significantly increases the specific surface area, facilitating oil adsorption by providing rapid infiltration pathways (microchannels) and abundant adsorption sites (nanopores) [7]. However, excessive PBAT content (70 wt%, PBAT-70%, Fig. 2h) leads to structural deterioration: large PBAT particles (1–5 μm) aggregate on the pore walls, reducing microscale pore diameters to <10 μm and causing partial blockage. The pore walls also become sticky due to the high mobility of PBAT's amorphous segments, further smoothing the surface. In the pure PBAT aerogel (Fig. 2i), the structure collapses, resulting in irregular, interconnected pores (5–20 μm) and the loss of the ordered honeycomb architecture observed in PLLA-rich composites. These findings highlight that a balanced PBAT content (50 wt%) optimally preserves the porous network while minimizing structural defects such as pore blockage and collapse, thereby underpinning the superior adsorption performance of PBAT-50% aerogels.

X-ray diffraction (XRD) analysis was conducted to investigate the crystalline structure of PLLA/PBAT composite aerogels with varying PBAT contents (pure PLLA to pure PBAT) (Fig. 3a). The pure PLLA aerogel exhibits a sharp peak at $2\theta = 16.8^\circ$, corresponding to the (110) crystal PLLAne of the α-crystalline form, indicative of the ordered packing of PLLA molecular chains [40]. In contrast, the pure PBAT aerogel disPLLAys broader diffraction peaks, characteristic of semicrystalline polymers, with five distinct peaks at $2\theta = 16.3^\circ$ (011), 17.5° (010), 20.5° (101), 23.4° (100), and 24.9° (111) [41]. These peaks arise from the aliphatic-aromatic copolymer segments in PBAT, which form less ordered crystals compared to PLLA. For composite aerogels (PBAT-30% to PBAT-70%), the α -crystalline peak of PLLA at $2\theta = 16.8^\circ$ is retained, but its intensity decreases with increasing PBAT content (e. g., 30% reduction in PBAT-50% vs. pure PLLA), suggesting that PBAT disrupts the regular arrangement of PLLA molecular chains and inhibits spherulite growth [42]. The XRD results confirm the coexistence of independent crystalline phases, which is consistent with a physical blending mechanism.

Fourier-transform infrared (FTIR) spectroscopy (Fig. 3b) further corroborates the absence of chemical reactions between PLLA and PBAT. Key characteristic peaks exhibit concentration-dependent trends: C—H stretching vibrations (2956.7 cm-1), dominant in PBAT due to its aliphatic adipate segments; peak intensity decreases with lower PBAT content [43]. Carbonyl (C=O) stretching at 1752.9 cm-1, a strong marker for PBAT (arising from terephthalate units); intensity scales linearly with PBAT loading, confirming proportional blending [44]. C-

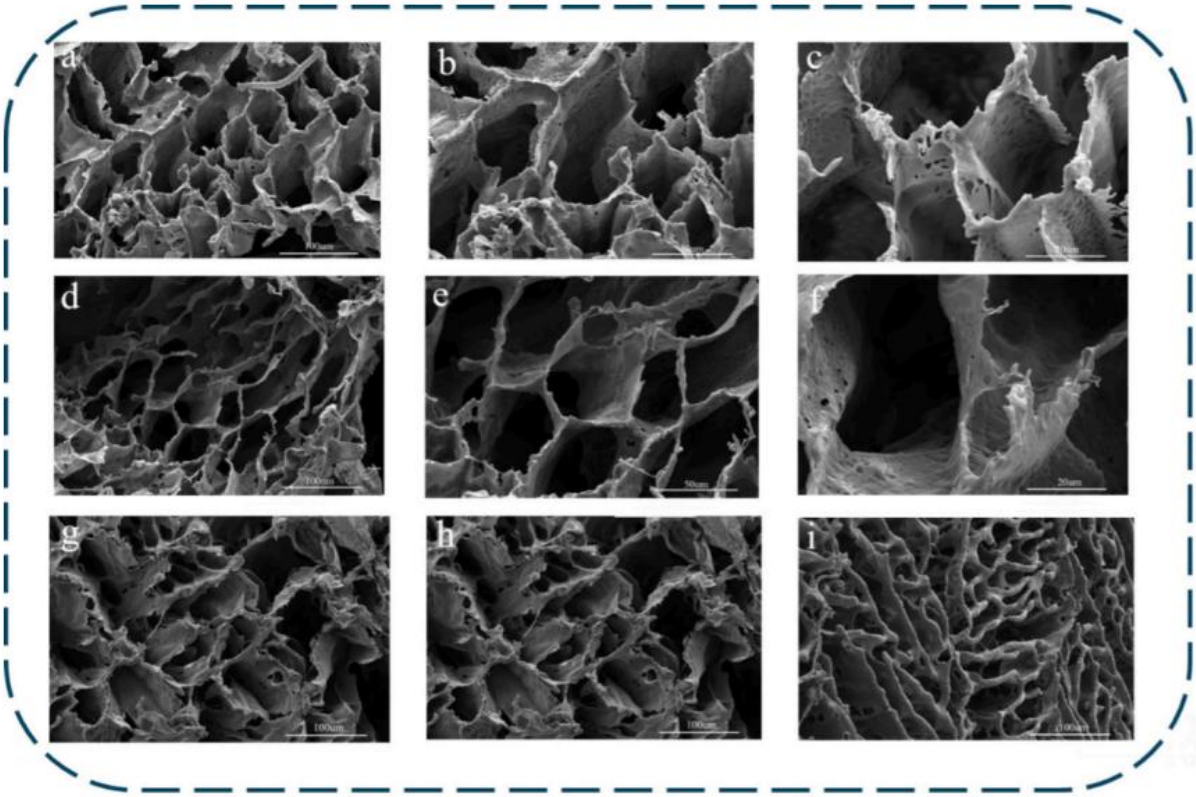

Fig. 2. SEM images of PLLA/PBAT composite aerogels with different PBAT contents added: (a, b, c) pure PLLA; (d, e, f) PBAT- 50%; (g) PBAT- 30%; (h) PBAT- 70%; (i) pure PBAT.

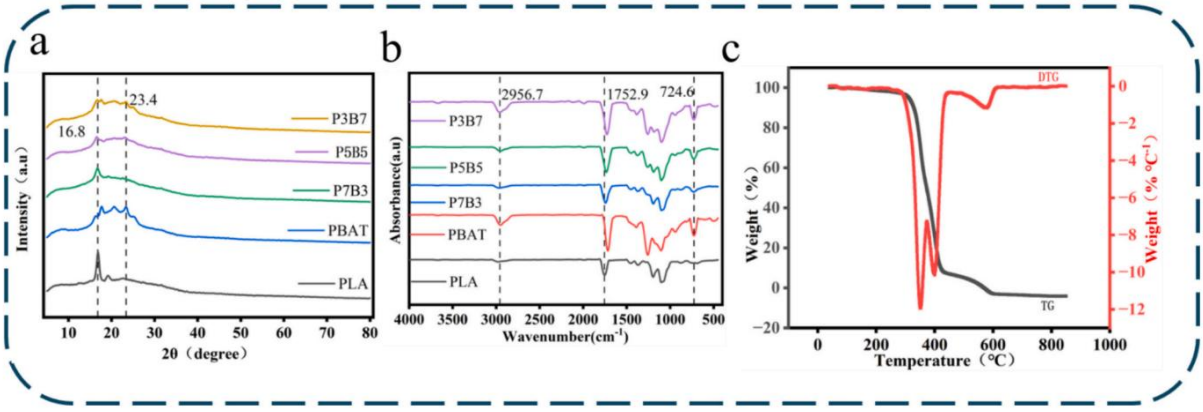

Fig. 3. (a) XRD spectra of PLLA/PBAT composite aerogels with varying PBAT contents (pure PLLA, 30%, 50%, 70%, and pure PBAT); (b) FTIR spectra of PLLA/PBAT composite aerogels with varying PBAT contents (pure PLLA, 30%, 50%, 70%, and pure PBAT); (c) Thermogravimetric (TG) and derivative thermogravimetric

(DTG) curves of the PBAT-50% aerogel.

O-C stretching at 1254.3 cm-1, present in both polymers but more intense in PBAT; intensity diminishes with reduced PBAT content. C—H out-of-PLLAne bending of PBAT's benzene ring at 724.6 cm-1, a signature peak unique to PBAT; peak intensity decreases with increasing PLLA content, vanishing in pure PLLA. Therefore, the intensity of these

peaks scales linearly with PBAT content, confirming proportional blending. No new peaks (e.g., ester linkages or crosslinking byproducts) indicative of chemical reactions are observed, confirming that PLLA and PBAT interact via physical mixing (hydrogen bonding between carbonyl groups and 1,4-dioxane residues) [37] [45].

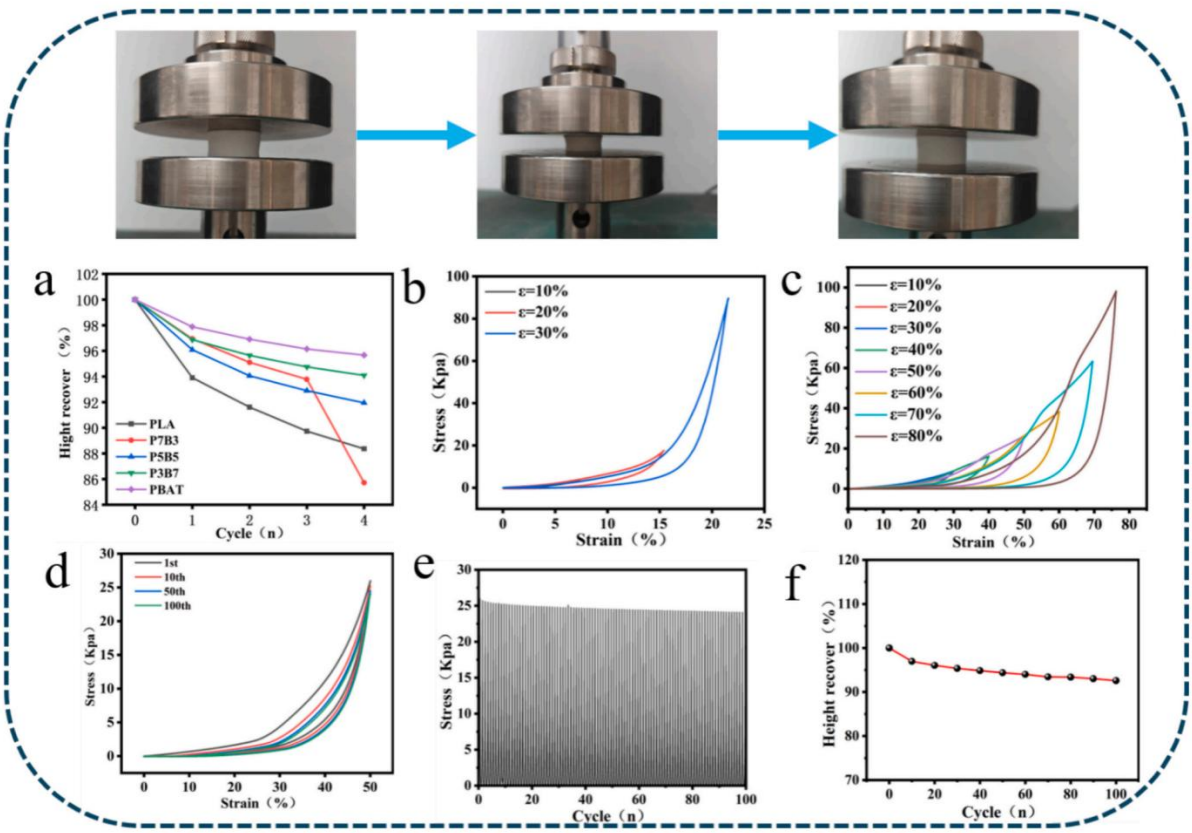

Fig. 4. (a) The high recovery rates of pure PLLA, PLLA/PBAT-30%%, PLLA/PBAT-50%%, PLLA/PBAT-70%% and pure PBAT after 4 compression cycles at 30% strain; (b, c) Compression strain-stress curves of pure PLLA and PLLA/PBAT-50%% at different strains (10%, 20%, 30% - 80%); (d) PLLA/PBAT-50%% compressed 100 times at a constant strain of 50%; (e) The high recovery rate of PLLA/PBAT-50%% after 100 cycles at a constant strain of 50%; (f) The stress of PLLA/PBAT-50%% after 100 cycles of compression at a constant strain of 50%.

The thermal stability of PBAT-50%% was investigated using thermogravimetric analysis (TG) and derivative thermogravimetric analysis (DTG) under a nitrogen atmosphere, as shown in Fig. 2c. A minor mass loss (~2.3%) observed below 100 ◦C is attributed to the evaporation of physically adsorbed water and residual 1,4-dioxane solvent entrapped within the porous network. The primary degradation phase initiates at approximately 300 ◦C, with the maximum degradation rate at 350 ◦C (DTG peak). This corresponds to the thermal cleavage of ester bonds in the polymer chains. The degradation process consists of two distinct stages: the first (300–380 ◦C) primarily involves PLLA decomposition, as its aliphatic ester linkages exhibit lower thermal stability compared to PBAT's aromatic-terephthalate moieties. The second stage (380–450 ◦C) is associated with PBAT degradation, consistent with the higher thermal stability of pure PBAT (onset degradation at ~400

◦C compared to ~350 ◦C for pure PLLA) [46]. Above 600 ◦C, PLLA undergoes complete thermal decomposition, leaving no residual mass, whereas PBAT leaves a small carbonaceous residue (~3.1%), attributed to partial coking and carbonization of its aromatic segments. Importantly, the incorporation of PBAT enhances the thermal stability of the composite, as evidenced by the onset degradation temperature of PBAT-50% (300 ◦C), which is 10 ◦C higher than that of pure PLLA. This improvement is indicative of a synergistic effect derived from the aromatic units of PBAT, which contribute to the retardation of chain scission.

3.2. Compressibility, elasticity, and fatigue resistance of PLLA/PBAT-X

The compressive performance of PLLA/PBAT aerogels was systematically evaluated to assess their structural stability under repeated compression, focusing on recovery rate, stress-strain behavior, and fatigue resistance. As shown in Fig. 4a, the height recovery rates of aerogels after 4 compression cycles at 30% strain exhibit significant variation with PBAT content. The pure PLLA aerogel exhibits a recovery rate of 88.4%, limited by its brittle nature, as the rigid crystalline PLLA network undergoes irreversible deformation under stress, leading to partial structural collapse [22]. In contrast, the recovery rate improves with increasing PBAT content: PBAT-30% (90.2%), PBAT-50% (92.0%), and PBAT-70% (91.5%), with pure PBAT aerogel achieving the highest recovery rate of 93.1%. This enhancement is attributed to the flexible aliphatic segments of PBAT, which act as “molecular springs” that dissipate compressive energy and facilitate network rebound, thereby mitigating irreversible deformation [47]. Among the composite aerogels, PBAT-50% achieves the highest recovery efficiency, balancing PLLA’s structural rigidity with PBAT’s elasticity. Insufficient PBAT content in PBAT-30% fails to establish a continuous flexible network, resulting in lower recovery rates, while excessive PBAT content in PBAT-70% leads to pore-wall adhesion during compression due to the stickiness of PBAT chains, slightly reducing recovery efficiency [48]. Stressstrain curves of pure PLLA (Fig. 4b) and PBAT-50% (Fig. 4c) at varying strains (10–80%) reveal distinct mechanical behaviors, divided into three regions: Linear elastic region ($\varepsilon \leq 30\%$): Characterized by a steep stress increase, corresponding to elastic buckling of the porous skeleton. PBAT-50% exhibits a lower initial modulus than pure PLLA, as PBAT’s flexibility reduces the overall stiffness of the network [49]. PLLAteau region ($30\% < \varepsilon < 70\%$): Stress increases gradually due to progressive collapse of microscale pores. PBAT-50% demonstrates a broader PLLAteau, indicating gradual deformation of PBAT-reinforced pore walls without abrupt fracture, unlike pure PLLA, which experiences sudden skeleton failure above 50% strain. Densification region ($\varepsilon \geq 70\%$): Stress rises sharply as pore walls come into contact. PBAT-50% sustains higher strains (up to 80%) than pure PLLA (≤60%), enabled by PBAT’s toughness, which prevents catastrophic cracking [50].

The incorporation of PBAT transforms the aerogel’s mechanical response from brittle (PLLA) to ductile (composite), which is critical for maintaining structural integrity under repeated compression. As depicted in Fig. 4d-f, at a strain of 50%, PLLA/PBAT-50% retains 92.9% of its stress after 100 compression cycles, with only a 7% drop, demonstrating exceptional fatigue resistance and ductile stress-strain behavior. This mechanical resilience directly supports the aerogel’s reusability in continuous oil-water separation applications. Unlike fragile fillermodified aerogels [35], PBAT-50% withstands repeated adsorptiondesorption cycles (via compression-induced oil extrusion), making it suitable for long-term environmental remediation applications.

3.3. Oil/water separation performance, sorption properties, and recyclability

The oil adsorption and separation performance of PLLA/PBAT aerogels was systematically assessed, focusing on porosity, hydrophobicity, and structural integrity. Porosity is a key determinant of adsorption capacity, as it provides the necessary void space for oil storage. As shown in Fig. 5a, the pure PLLA aerogel exhibits the highest porosity (98.6% ± 0.3%), attributed to its well-developed honeycomb-like network (Fig. 2). With increasing PBAT content, the porosity gradually decreases to 97.8% (PBAT-30%), 96.5% (PBAT-50%), 95.2% (PBAT-70%), and 94.1% (PBAT). This reduction is primarily due to the high viscosity of PBAT, which

partially blocks the pores of PLLA during phase separation, consistent with SEM observations of pore narrowing in aerogels with high PBAT content (Fig. 2i). Water contact angle (WCA) measurements further illustrate the surface hydrophobicity of aerogels (Fig. 5b). The pure PLLA aerogel exhibits a WCA of 116.8◦ ± 1.2◦, indicative of hydrophobic surfaces due to its low surface energy and rough pore walls. With the incorporation of PBAT, the WCAs gradually decrease: 108.5◦ ± 1.5◦ (PBAT-30%), 102.3◦ ± 1.1◦ (PBAT-50%), 95.7◦ ± 0.9◦ (PBAT-70%), and 89.2◦ ± 1.3◦ (PBAT). This trend reflects the higher polarity of PBAT, whose molecular chain contains more ester and hydroxyl groups than PLLA, increasing surface energy and reducing hydrophobicity. Notably, PBAT-50% maintains moderate hydrophobicity (WCA = 102.3◦), achieving an optimal balance between porosity and surface properties for effective oil-water selectivity. The underwater stability of PBAT-50% was validated via immersion tests (Fig. 5c). After 24 h of submersion in deionized water, the aerogel retained 99.6% of its initial mass, indicating negligible water absorption. The aerogel surface exhibited a distinct silver mirror-like appearance, characteristic of the Cassie-Baxter nonwetting state. In this state, an air layer trapped at the interface between the aerogel surface and water prevents direct liquidsolid contact, thereby enabling selective oil adsorption [41]. This property is essential for practical applications, as it ensures the aerogel retains its hydrophobicity in aqueous environments. Fig. 5d illustrates the n-hexane adsorption capacities of PLLA/PBAT aerogels with varying PBAT contents. The composite aerogels, benefiting from their hierarchical nanoporous structure and optimized surface hydrophobicity, exhibit excellent solvent adsorption performance. The pure PLLA aerogel adsorbs n-hexane with a capacity of 12.3 g/g, which increases with PBAT content, reaching a peak of 13.6 g/g for PBAT-50% (50 wt% PBAT). This improvement is attributed to the hierarchical porosity of PBAT-50%, which features interconnected microscale channels (15–40 μm) that facilitate rapid oil infiltration via capillary action. Additionally, the nanoscale pores (50–200 nm) on the pore walls significantly increase the specific surface area, providing abundant adsorption sites for oil molecules.

Despite the slight reduction in water contact angle (102.3◦ for PBAT-50% compared to 116.8◦ for pure PLLA), PBAT-50% achieves a balanced surface energy that promotes oil-phase wetting while avoiding excessive hydrophilicity-induced water adsorption, which is critical for selective oil capture in aqueous environments. Beyond n-hexane, PBAT-50% PLLA/PBAT aerogel demonstrates excellent adsorption capabilities for various oils and organic solvents. As shown in Fig. 5e, the adsorption capacity of PBAT-50% exceeds 15.0 g/g for all tested liquids including carbon tetrachloride (31.5 g/g), acetone (22.8 g/g), toluene (19.7 g/g), pump oil (18.2 g/g), olive oil (17.5 g/g), and 18# gear oil (16.3 g/g). The remarkably high adsorption capacity for carbon tetrachloride can be attributed to its high density (1.59 g/cm3), which accelerates infiltration

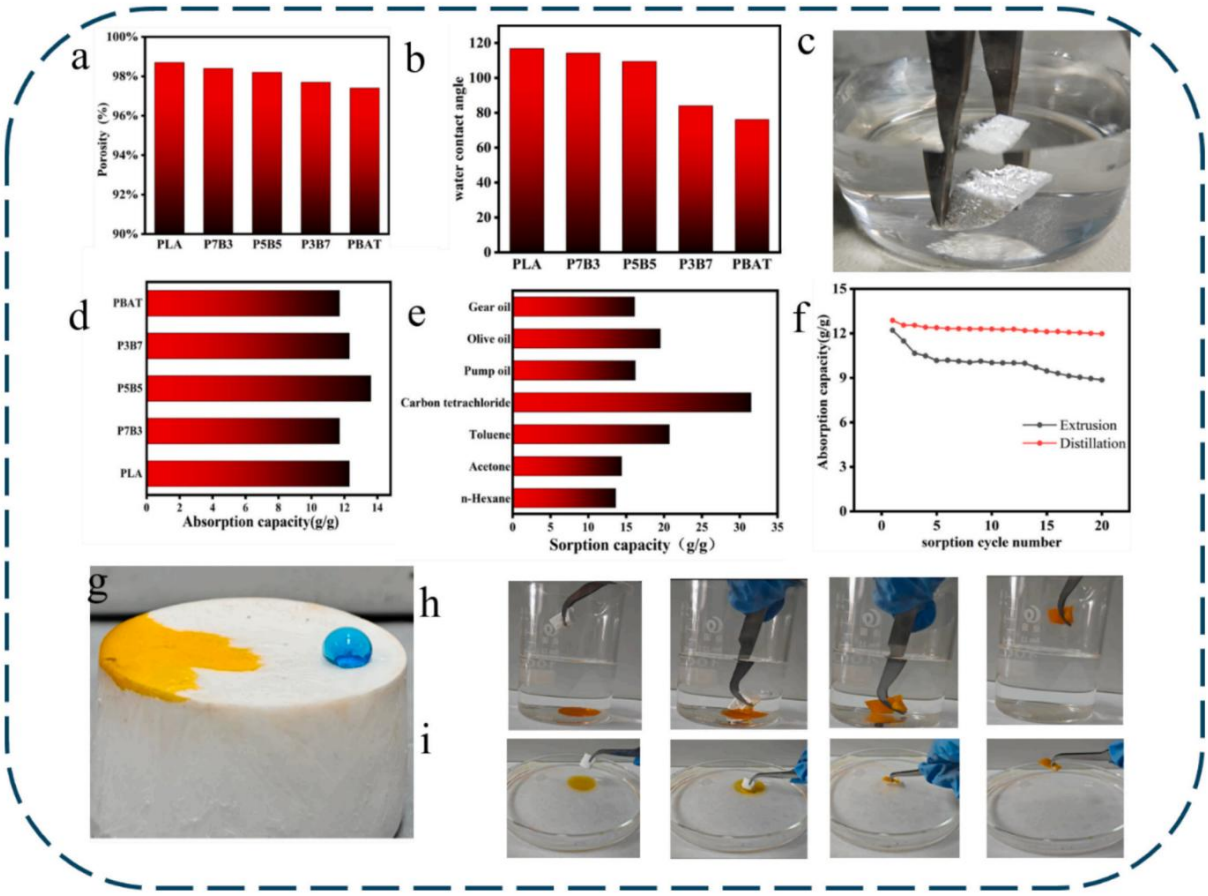

Fig. 5. (a) Porosity and (b) water contact angle (WCA) of PLLA/PBAT aerogels with varying PBAT contents; (c) Digital image of PBAT-50% aerogel submerged in water. (d) n-Hexane adsorption capacities of PLLA/PBAT aerogels with different PBAT ratios. (e) Adsorption capacities of PBAT-50% aerogel for various oils and organic solvents; (f) Cyclic adsorption capacity of PBAT-50%% aerogel for n-hexane via extrusion and distillation; (g) Schematic illustration of selective oil/water wetting behavior on the surface of PBAT-50%% (oil: red, water: blue). (h) Underwater adsorption process of carbon tetrachloride (dyed with Sudan I) by PBAT-50%; and (i) Dynamic adsorption curve of n-hexane (dyed with Sudan I) on water surface using PBAT-50%. (For interpretation of the references to colour in this figure legend, the reader is referred to the web version of this article.)

into the aerogel's porous network via gravity-driven flow. All tested liquids, including carbon tetrachloride, acetone, toluene, pump oil, olive oil, gear oil, and n-hexane, achieved adsorption capacities exceeding 15.0 times the weight of the 50 wt% PLLA/PBAT composite aerogel. Notably, the adsorption capacity for carbon tetrachloride was up to 31.5 times higher. The adsorption mechanism is primarily governed by physisorption, which includes capillary action (facilitated by the aerogel's porous structure) and van der Waals interactions between oil molecules and the polymer matrix. Weak chemisorption, such as hydrogen bonding between polar groups in oils (e.g., ester groups in olive oil) and the aerogel's carbonyl/ether groups, PLLAys a secondary role but does not significantly diminish the dominant contribution of physisorption.

The reusability of PBAT-50% was evaluated via two regeneration methods: compression-induced oil extrusion and distillation (Fig. 5f). After 20 adsorption-desorption cycles, the aerogel retained 85.2% of its initial n-hexane adsorption capacity (11.6 g/g), Compression at 50% strain, which is more practical for on-site regeneration, removed approximately 80% of the adsorbed oil via physical extrusion. In contrast, distillation at 80 °C for 2 h achieved a more thorough regeneration, removing approximately 95% of the adsorbed oil. This remarkable cycling stability can be attributed to the mechanical

resilience of PBAT-50% (Fig. 3), which enables it to recover its shape after compression, thereby preserving the integrity of its porous structure and maintaining efficient oil-uptake pathways over repeated cycles. The selective hydrophobic-lipophilic properties of PBAT-50% were visually demonstrated by depositing water (dyed with methylene blue) and n-hexane (dyed with Sudan I) droplets on its surface (Fig. 6g). The n-hexane droplet was completely absorbed within 1.3 s, while the water droplet remained intact with a contact angle of $102.3^{\circ} \pm 1.1^{\circ}$, demonstrating efficient oil-water discrimination. This selectivity arises from the aerogel's hierarchical porosity and balanced surface energy, which promote rapid oil infiltration while repelling water. As shown in Figs. 5 h and 5i, PBAT-50%% can efficiently adsorb n-hexane (Sudan I dye) floating on the water surface and CCl4 (Sudan I dye) underwater, leaving clean water.

The practical utility of PBAT-50%% for large-scale oil-water separation was evaluated using a gravity-driven setup (Fig. 6a–b). For both light oil (n-hexane/water) and heavy oil (CCl4/water) mixtures, the aerogel functioned as a filtration membrane, enabling rapid, passive separation without external energy input. A 40 mL CCl4/water mixture (1:1 ν /v) was completely separated in 49 s, corresponding to an ultrahigh flux of 7855.5 L·m-2·h-1 (calculated based on the aerogel's effective area). This high flux is attributed to the aerogel's interconnected

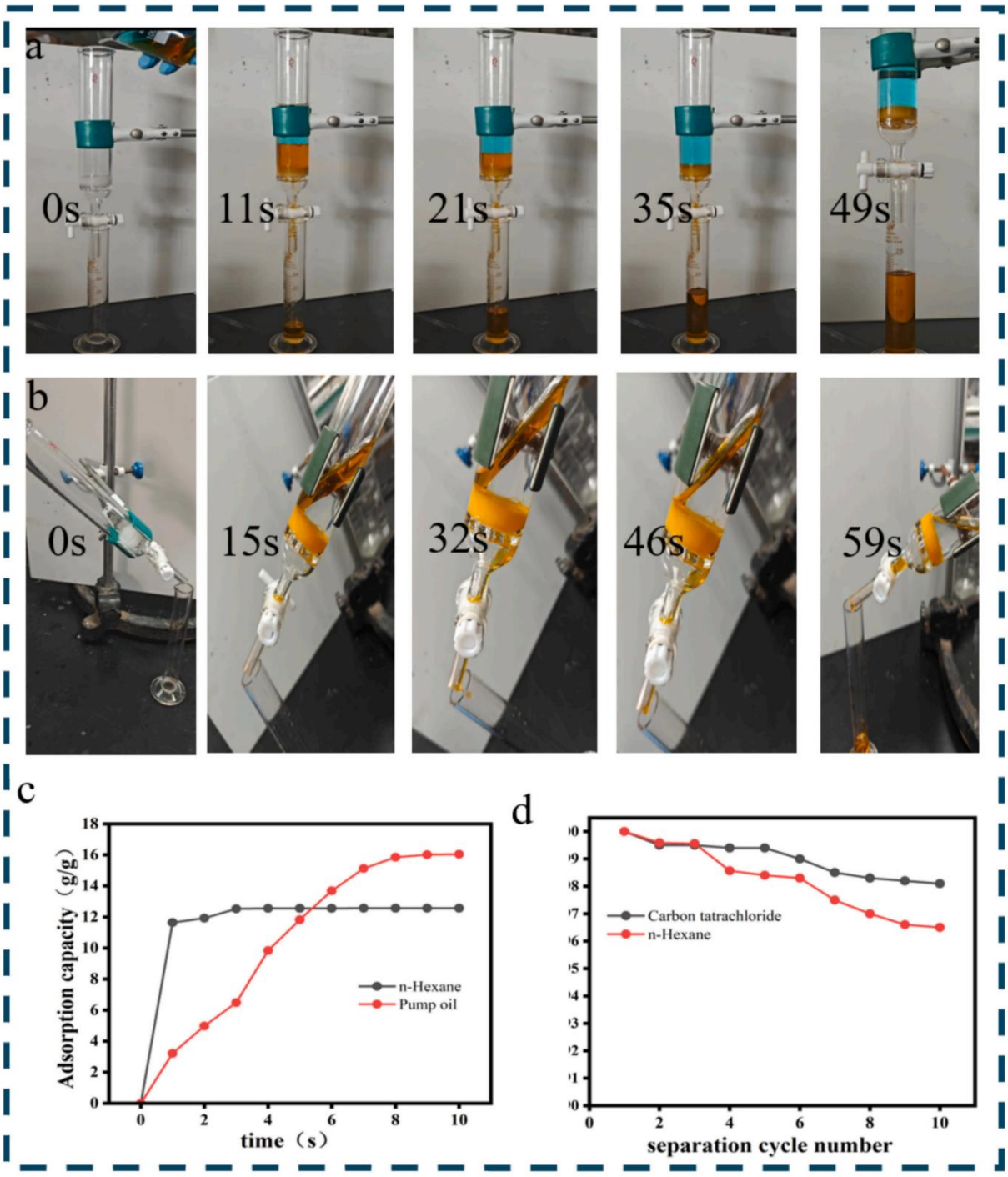

Fig. 6. Photograph of continuous separation of (a) carbon tetrachloride (b) hexane under gravity. (c) Kinetic plot of PBAT-50%% adsorption of hexane and pump oil (d) Cyclic separation performance of PBAT-50%%.

macropores (10–50 μm), which act as channels for rapid oil permeation. For CCl□/water, the efficiency reached 99.59% ± 0.21%, with no detectable water in the collected oil phase (verified by Karl Fischer titration). For n-hexane/water, the efficiency was 98.7% ± 0.35%, confirming consistent performance across different oil densities. Adsorption kinetic curves (Fig. 6c) show that PBAT-50% reaches adsorption equilibrium within 30 min for n-hexane (13.6 g/g) and 45 min for pump oil (18.2 g/g). Cyclic separation tests (Fig. 6d) revealed that the separation efficiency remains above 96.5% after 20 cycles, with only a 3.2% decrease

in flux. Combined with its biodegradability and cost-effective fabrication process, PBAT-50%'s high flux, separation efficiency, and recyclability make it a promising material for large-scale oily wastewater remediation and oil spill cleanup.

4. Conclusions

PLLA/PBAT composite aerogels with hierarchical porous structures were successfully fabricated via freeze-drying and solvent-induced phase separation, using 1.4-dioxane as a co-solvent to address the inherent incompatibility between PLLA and PBAT. Notably, the optimal PBAT-50 aerogel can retain 92.0% of its height after four compression cycles at 30% strain and 92.9% stress retention after 100 cycles at 50% strain, effectively addressing the inherent brittleness of PLLA-based materials. Beyond mechanical robustness, its adsorption capacities vary from 13.6 to 31.5 g/g for various oils and organic solvents, with over 98.7% gravity-driven oil-water separation efficiency, and an ultrahigh flux of 7855.5 $L \cdot m^{-2} \cdot h^{-1}$. Moreover, 76–80.67% adsorption capacity can be retained after 10 regeneration cycles. Its selective hydrophobic-lipophilic behavior and underwater stability further support its utility in oil spill remediation and oily wastewater treatment. This study provides a sustainable, high-performance material bridging material science and environmental engineering, offering a practical solution for oil-contaminated water remediation.

CRediT authorship contribution statement

Xinkai Sun: Writing – original draft. Xinying Jiang: Investigation. Fei Xie: Software. Pengju Yao: Visualization. Yi Zhang: Resources. Hui Yang: Software. Carla Bittencourt: Supervision. Wenjiang Li: Writing – review & editing.

Declaration of competing interest

The authors declare that they have no known competing financial interests or personal relationships that could have appeared to influence the work reported in this paper.

Acknowledgements

This work was supported by Tianjin University of Technology - Yulin City (Xingye) Calcium-based Materials Research Center; CB thanks the Belgian Fund for Scientific Research under the FRFC contract CDR J001019. CB is a Senior Researcher of the National Funds for Scientific Research (FRS-FNRS, Belgium).

Appendix A. Supplementary data

Supplementary data to this article can be found online at https://doi.org/10.1016/j.ijbiomac.2026.150327.

Data availability

Data will be made available on request.

References

- W. Qu, Z. Wang, X. Wang, Z. Wang, D. Yu, D. Ji, High-hydrophobic ZIF-67@PLA honeycomb aerogel for efficient oil-water separation, Colloids Surf. A Physicochem. Eng. Asp. 658 (2023), https://doi.org/10.1016/j. colsurfa.2022.130768.
- [2] X. Li, T. Liu, Y. Zhang, J. Cai, M. He, M. Li, Z. Chen, L. Zhang, Growth of BiOBr/ZIF-67 nanocomposites on carbon Fiber cloth as filter-membrane-shaped Photocatalyst for degrading pollutants in flowing wastewater, Adv. Fiber Mater. 4 (6) (2022) 1620–1631, https://doi.org/10.1007/s42765-022-00189-w.
- [3] M. Liu, J. Chen, X. Cai, Y. Han, S. Xiong, Oil–water pre-separation with a novel axial hydrocyclone, Chin. J. Chem. Eng. 26 (1) (2018) 60–66, https://doi.org/ 10.1016/j.cjche.2017.06.021.

- [4] C.Y. Teh, P.M. Budiman, K.P.Y. Shak, T.Y. Wu, Recent advancement of coagulation-flocculation and its application in wastewater treatment, Ind. Eng. Chem. Res. 55 (16) (2016) 4363–4389, https://doi.org/10.1021/acs.iecr.5b04703.
- [5] C. Wan, Y. Jiao, S. Wei, X. Li, W. Tian, Y. Wu, J. Li, Scalable top-to-bottom design on low tortuosity of anisotropic carbon aerogels for fast and reusable passive capillary absorption and separation of organic leakages, ACS Appl. Mater. Interfaces 11 (51) (2019) 47846–47857, https://doi.org/10.1021/acsami.9b13686.
- [6] H. Sai, R. Fu, L. Xing, J. Xiang, Z. Li, F. Li, T. Zhang, Surface modification of bacterial cellulose aerogels' web-like skeleton for oil/water separation, ACS Appl. Mater. Interfaces 7 (13) (2015) 7373–7381, https://doi.org/10.1021/ acsami 5b00846
- [7] P.S. Jadhav, A. Sarkar, S. Pasupathy, S. Ren, Biogenic straw aerogel thermal insulation materials, Adv. Eng. Mater. 25 (13) (2023), https://doi.org/10.1002/ adem 202300037
- [8] X. Shi, X. Fan, Y. Zhu, Y. Liu, P. Wu, R. Jiang, B. Wu, H.-A. Wu, H. Zheng, J. Wang, X. Ji, Y. Chen, J. Liang, Pushing detectability and sensitivity for subtle force to new limits with shrinkable nanochannel structured aerogel, nature, Communications 13 (1) (2022), https://doi.org/10.1038/s41467-022-28760-4.
- [9] A. Varamesh, Y. Zhu, G. Hu, H. Wang, H. Rezania, Y. Li, Q. Lu, X. Ren, F. Jiang, S. L. Bryant, J. Hu, Fully biobased thermal insulating aerogels with superior fire-retardant and mechanical properties, Chem. Eng. J. 495 (2024), https://doi.org/10.1016/j.cei.2024.153587.
- [10] Y. Wang, H. Li, Y. Xie, X. Li, S. Sun, X. Jing, H.-Y. Mi, Y. Wang, C. Liu, C. Shen, Regulating microstructures of aerogels by controlling phase separation mechanism for improving specific surface area and energy harvesting, J. Colloid Interface Sci. 658 (2024) 772–782, https://doi.org/10.1016/j.jcis.2023.12.072.
- [11] N. Zion, J.C. Douglin, D.A. Cullen, P. Zelenay, D.R. Dekel, L. Elbaz, Porphyrin aerogel catalysts for oxygen reduction reaction in anion-exchange membrane fuel cells, Adv. Funct. Mater. 31 (24) (2021), https://doi.org/10.1002/ adfm 202100963
- [12] Z.M. Han, W.B. Sun, K.P. Yang, H.B. Yang, Z.X. Liu, D.H. Li, C.H. Yin, H.C. Liu, Y. X. Zhao, Z.C. Ling, Q.F. Guan, S.H. Yu, An all-natural wood-inspired aerogel, Angew. Chem. Int. Ed. 62 (6) (2022), https://doi.org/10.1002/anie.202211099.
- [13] W. Qu, Z. Wang, M. Qin, X. Yang, F. Zhang, Z. Wang, D. Ji, D. Yu, Synthesis and characterization of UiO-66-NH2 incorporated PVA/cellulose nanofibers composite aerogel for enhanced oil-water separation and formaldehyde adsorption, Sep. Purif. Technol. 325 (2023), https://doi.org/10.1016/j.seppur.2023.124673.
- [14] X. Shan, L. Liu, Y. Wu, D. Yuan, J. Wang, C. Zhang, J. Wang, Aerogel-functionalized thermoplastic polyurethane as waterproof, breathable freestanding films and coatings for passive daytime radiative cooling, advanced, Science 9 (20) (2022), https://doi.org/10.1002/advs.202201190.
- [15] T. Wang, W. Wang, C. Hu, J. Zheng, B. Liu, Z. Zhu, Mechanically durable, recyclable polyvinyl alcohol/lignin-based aerogel for efficient oil/water separation and solar-powered removal of high-viscosity oil, Ind. Crop. Prod. 219 (2024), https://doi.org/10.1016/j.indcrop.2024.119131.
- [16] Z. Zheng, T. Shi, H. Liu, D. Wu, X. Wang, Polyimide/phosphorene hybrid aerogel-based composite phase change materials for high-efficient solar energy capture and photothermal conversion, Appl. Therm. Eng. 207 (2022), https://doi.org/10.1016/i.applthermaleng.2022.118173.
- [17] J. Zhou, R. Zhang, R. Xu, Y. Li, W. Tian, M. Gao, M. Wang, D. Li, X. Liang, L. Xie, K. Liang, P. Chen, B. Kong, Super-assembled hierarchical cellulose aerogel-gelatin solid electrolyte for implantable and biodegradable zinc ion battery, Adv. Funct. Mater. 32 (21) (2022), https://doi.org/10.1002/adfm.202111406.

- [18] J. Yuan, X. Gao, Y. Chen, L. Zhao, D. Hu, Green fabrication of biobased and degradable poly(lactic acid)/poly(butylene succinate) open-cell foams for highly efficient oil-water separation with ultrafast degradation, ACS Sustain. Chem. Eng. 12 (50) (2024) 18101–18113, https://doi.org/10.1021/acssuschemeng.4c06545.
- [19] M. Arrieta, M. Samper, M. Aldas, J. López, On the use of PLA-PHB blends for sustainable food packaging applications, Materials 10 (9) (2017), https://doi.org/ 10.3390/ma10091008
- [20] Z. Gong, Y. Chen, J. Yuan, L. Zhao, D. Hu, Shape memory temperature-tunable poly (butylene adipate-co-terephthalate)/Polylactic acid foams prepared by supercritical CO2 foaming, ACS Sustain. Chem. Eng. 12 (32) (2024) 12064–12075, https://doi.org/10.1021/acssuschemeng.4c03546.
- [21] H. Liu, P. Chen, Q. Peng, D. Bai, Ultralight, superhydrophobic and biodegradable stereocomplex polylactide aerogel with superior oil-water separation and thermal insulation performances, Ind. Crop. Prod. 222 (2024), https://doi.org/10.1016/j. indcrop.2024.119983.
- [22] J. Beauson, G. Schillani, L. Van der Schueren, S. Goutianos, The effect of processing conditions and polymer crystallinity on the mechanical properties of unidirectional self-reinforced PLA composites, Compos. A: Appl. Sci. Manuf. 152 (2022), https:// doi.org/10.1016/j.compositesa.2021.106668.
- [23] J. Chen, C. Rong, T. Lin, Y. Chen, J. Wu, J. You, H. Wang, Y. Li, Stable co-continuous PLA/PBAT blends Compatibilized by interfacial Stereocomplex crystallites: toward full biodegradable polymer blends with simultaneously enhanced mechanical properties and crystallization rates, Macromolecules 54 (6) (2021) 2852–2861, https://doi.org/10.1021/acs.macromol.0c02861.
- [24] X. Zhao, J. Liu, J. Li, X. Liang, W. Zhou, S. Peng, Strategies and techniques for improving heat resistance and mechanical performances of poly(lactic acid) (PLA) biodegradable materials, Int. J. Biol. Macromol. 218 (2022) 115–134, https://doi. org/10.1016/j.ijbiomac.2022.07.091.
- [25] L.J. Jia, A.D. Phule, Z. Yu, X. Zhang, Z.X. Zhang, Ultra-light poly(lactic acid)/SiO2 aerogel composite foam: a fully biodegradable and full life-cycle sustainable insulation material, Int. J. Biol. Macromol. 192 (2021) 1029–1039, https://doi.org/10.1016/j.ijbiomac.2021.10.053.
- [26] L. Jing, P. Zhang, Y. Chen, Y. Gao, J. Yun, Preparation of superhydrophobic PDMS/ DTMS-SiO2@PLA membrane for oil-water separation with three-dimensional layered porous structure by simple spraying, Colloids Surf. A Physicochem. Eng. Asp. 688 (2024), https://doi.org/10.1016/j.colsurfa.2024.133601.
- [27] S. Liao, D. Bai, Y. Jia, J. Sun, H. Liu, L. Li, M. Xu, Superhydrophobic stereocomplextype polylactide/ultra-fine glass fibers aerogel for passive daytime radiative cooling, Int. J. Biol. Macromol. 274 (2024), https://doi.org/10.1016/j. ijbiomac.2024.133470.
- [28] J. Mo, Y. Wang, J. Lin, Y. Ke, C. Zhou, J. Wang, J. Wen, F. Gan, L. Wang, C. Ma, Polylactic acid/multi-wall carbon nanotubes composite fibrous membrane and their applications in oil-water separation, Surf. Interfaces 39 (2023), https://doi. org/10.1016/j.surfin.2023.102908.
- [29] H. Jia, Y. Hou, M. Zhang, Y. Pan, C. Liu, C. Shen, X. Liu, SC crystals of porous PLA via thermally–induced phase separation: effects of process conditions, solvent composition and nucleating agent, Eur. Polym. J. 213 (2024), https://doi.org/ 10.1016/j.eurpolymj.2024.113095.
- [30] Y. Zhang, J. Guo, J. Sun, F. Guan, J. Tao, X. Song, Z. Li, Bilayer fiber membrane electrospun from polylactic acid/alginate/bromelain and polylactic acid for enhancing the functionality of tea bags, Int. J. Biol. Macromol. 260 (2024), https:// doi.org/10.1016/j.ijbiomac.2024.129449.
- [31] B. Li, G. Zhao, G. Wang, L. Zhang, J. Gong, Z. Shi, Biodegradable PLA/PBS opencell foam fabricated by supercritical CO2 foaming for selective oil-adsorption, Sep. Purif. Technol. 257 (2021),https://doi.org/10.1016/j.seppur.2020.117949.
- [32] X. Gong, L. Zhang, Y. Liu, M. Zhu, A review on zeolitic imidazolate framework-8 based materials with special wettability for oil/water separation, journal of environmental, Chem. Eng. 11 (6) (2023), https://doi.org/10.1016/j. jece.2023.111360.

- [33] S. Zhang, Q. Zhang, X. Huang, X. Ning, J. Ming, Robust structure and superhydrophobic PLA/ZrO2 fiber aerogel for daytime radiative cooling, Advanced Industrial and Engineering Polymer Research (2025), https://doi.org/10.1016/j. aiepr.2025.10.001.
- [34] N. Iqbal, W. Tan, Q. Zhang, D. Iqbal, M.I. Hossen, G. Dou, X. Ning, J. Ming, PLA/ AgNPs fiber aerogels and its investigation into their antibacterial properties, J. Mol. Struct. 1317 (2024), https://doi.org/10.1016/j.molstruc.2024.139189.
- [35] Z.-M. Zhang, Z.-Q. Gan, R.-Y. Bao, K. Ke, Z.-Y. Liu, M.-B. Yang, W. Yang, Green and robust superhydrophilic electrospun stereocomplex polylactide membranes: multifunctional oil/water separation and self-cleaning, J. Membr. Sci. 593 (2020), https://doi.org/10.1016/j.memsci.2019.117420.
- [36] W. Zhang, Y. Liu, F. Tao, Y. An, Y. Zhong, Z. Liu, Z. Hu, X. Zhang, X. Wang, An overview of biomass-based oil/water separation materials, Sep. Purif. Technol. 316 (2023), https://doi.org/10.1016/j.seppur.2023.123767.
- [37] S. Khatsee, D. Daranarong, W. Punyodom, P. Worajittiphon, Electrospinning polymer blend of PLA and PBAT: Electrospinnability–solubility map and effect of polymer solution parameters toward application as antibiotic-carrier mats, J. Appl. Polym. Sci. 135 (28) (2018), https://doi.org/10.1002/app.46486.
- [38] Y. Guan, B. Bi, D. Qiao, S. Cao, W. Zhang, Z. Wang, H. Zeng, Y. Li, Bioinspired superhydrophobic polylactic acid aerogel with a tree branch structure for the removal of viscous oil spills assisted by solar energy, J. Mater. Chem. A 12 (16) (2024) 9850–9862, https://doi.org/10.1039/d4ta00349g.
- [39] B. Dong, P. Yao, F. Xie, H. Yang, R. Arenal, W. Li, Kapok/regenerated cellulose based carbon aerogel prepared at a low-temperature carbonization for oil/water separation, Ind. Crop. Prod. 222 (2024), https://doi.org/10.1016/j. indcrop.2024.119743.
- [40] W.-J. Hu, Q.-Q. Xia, H.-T. Pan, H.-Y. Chen, Y.-X. Qu, Z.-Y. Chen, G.-D. Zhang, L. Zhao, L.-X. Gong, C.-G. Xue, L.-C. Tang, Green and rapid preparation of fluorosilicone rubber foam materials with tunable chemical resistance for efficient oil–water separation, Polymers 14 (8) (2022), https://doi.org/10.3390/polym14081628.
- [41] M. Dilamian, B. Noroozi, Rice straw Agri-waste for water pollutant adsorption: relevant mesoporous super hydrophobic cellulose aerogel, Carbohydr. Polym. 251 (2021), https://doi.org/10.1016/j.carbpol.2020.117016.
- [42] M. Hua, D. Chen, Z. Xu, Y. Fang, Y. Song, Fabrication of high-expansion, fully degradable polylactic acid-based foam with exponent oil/water separation, J. Appl. Polym. Sci. 139 (48) (2022), https://doi.org/10.1002/app.53234.
- [43] H. Zhou, R. Meng, L. Wang, M. Zhu, X. Wei, X. Wang, J. Hu, Preparation of opencell chain-extend poly (lactic acid)/poly (butylene adipate-co-terephthalate) foams and their selective oil absorption characteristics, J. Supercrit. Fluids 204 (2024), https://doi.org/10.1016/j.supflu.2023.106114.
- [44] R. Zhan, X.-L. Li, Y. Zheng, X.-R. Zeng, L.-Y. Shi, K.-K. Yang, Y.-Z. Wang, Fabrication of high-strength and tough PLA/PBAT composites via in-situ copolymer formation using an adaptable epoxy extender, Int. J. Biol. Macromol. 302 (2025), https://doi.org/10.1016/j.ijbiomac.2025.140530.
- [45] W. Liu, Y. Wang, S. Xiang, H. Liu, Unveiling the effect of enhanced interfacial compatibility on the mechanical properties of PLA/PBAT blends, Polymer 296 (2024), https://doi.org/10.1016/j.polymer.2024.126815.
- [46] M. Bianchi, A. Dorigato, M. Morreale, A. Pegoretti, Evaluation of the physical and shape memory properties of fully biodegradable poly(lactic acid) (PLA)/Poly (butylene adipate terephthalate) (PBAT), Blends, Polymers 15 (4) (2023), https:// doi.org/10.3390/polym15040881.
- [47] H.-Y. Mi, X. Jing, Y. Liu, L. Li, H. Li, X.-F. Peng, H. Zhou, Highly durable Superhydrophobic polymer foams fabricated by extrusion and supercritical CO2 foaming for selective oil absorption, ACS Appl. Mater. Interfaces 11 (7) (2019) 7479–7487, https://doi.org/10.1021/acsami.8b21858.

- [48] X. Wang, Y. Pan, X. Liu, H. Liu, N. Li, C. Liu, D.W. Schubert, C. Shen, Facile fabrication of superhydrophobic and eco-friendly poly(lactic acid) foam for oil–water separation via skin peeling, ACS Appl. Mater. Interfaces 11 (15) (2019) 14362–14367, https://doi.org/10.1021/acsami.9b02285.
- [49] T. Krasian, W. Punyodom, P. Worajittiphon, A hybrid of 2D materials (MoS2 and WS2) as an effective performance enhancer for poly(lactic acid) fibrous mats in oil adsorption and oil/water separation, Chem. Eng. J. 369 (2019) 563–575, https:// doi.org/10.1016/j.cej.2019.03.092.
- [50] Y. Li, Z. Lin, X. Wang, Z. Duan, P. Lu, S. Li, D. Ji, Z. Wang, G. Li, D. Yu, W. Liu, High-hydrophobic ZIF-8@PLA composite aerogel and application for oil-water separation, Sep. Purif. Technol. 270 (2021), https://doi.org/10.1016/j. seppur.2021.118794.
- [51] B. Li, X. Ma, G. Zhao, G. Wang, L. Zhang, J. Gong, Green fabrication method of layered and open-cell polylactide foams for oil-sorption via pre-crystallization and supercritical CO2-induced melting, J. Supercrit. Fluids 162 (2020), https://doi. org/10.1016/j.supflu.2020.104854.
- [52] X. Chen, Y.N. Liang, X.-Z. Tang, W. Shen, X. Hu, Additive-free poly (vinylidene fluoride) aerogel for oil/water separation and rapid oil absorption, Chem. Eng. J. 308 (2017) 18–26, https://doi.org/10.1016/j.cej.2016.09.038.
- [53] J. Zhao, C. Xiao, N. Xu, Evaluation of polypropylene and poly (butylmethacrylateco-hydroxyethylmethacrylate) nonwoven material as oil absorbent, Environ. Sci. Pollut. Res. 20 (6) (2012) 4137–4145, https://doi.org/10.1007/s11356-012-1397- 8.
- [54] Y. Tong, Y. Li, Y. Li, H. Gao, Y. Weng, Anisotropically structured hydrophobic fungus aerogels for high-efficiency oil/water separation, Sustain. Mater. Technol. 45 (2025), https://doi.org/10.1016/j.susmat.2025.e01495.
- [55] M.W. Nugraha, M.D.H. Wirzal, F. Ali, L. Roza, N.S. Sambudi, Electrospun polylactic acid/ tungsten oxide/ amino-functionalized carbon quantum dots (PLA/WO3/N-CQDs) fibers for oil/water separation and photocatalytic decolorization, journal of environmental, Chem. Eng. 9 (5) (2021), https://doi.org/10.1016/j. jece.2021.106033.